Use of a portable MRI to evaluate root structure-function relationships in water-use for several herbaceous species

Magali Nuixe, Amidou Sissou Traoré, Shannan Blystone, J.-M. Bonny, Guilhem Pagès, Catherine Picon-Cochard

Original article

Title

Use of a portable MRI to evaluate root structure-function relationships in water-use for several herbaceous species

Authors information

Magali Nuixe[1,2,3], Amidou Sissou Traoré[1,2], Shannan Blystone[1,2,4], Jean-Marie Bonny[1,2], Guilhem Pagés[1,2] and Catherine Picon-Cochard[3,*]

[1] Université Clermont Auvergne, INRAE, UR QuaPA, F-63122 Saint-Genès-Champanelle, France.

[2] INRAE, PROBE research infrastructure, AgroResonance facility, F-63122 Saint-Genès-Champanelle, France.

[3] Université Clermont Auvergne, INRAE, VetAgro Sup, UREP, 63000 Clermont-Ferrand, France.

[4] Université Clermont Auvergne, INRAE, UMR PIAF, 63000 Clermont-Ferrand, France.

[*] Correspondence should be addressed to catherine.picon-cochard@inrae.fr, Tel.: +33(0)-443-761-615 (C.P.-C.).

ORCID numbers

M.N.: https://orcid.org/0000-0003-0960-8525

A.S.T.: https://orcid.org/0000-0002-3574-3475

S.B.: https://orcid.org/0000-0002-8494-2411

J.-M.B.: https://orcid.org/0000-0003-2858-7459

G.P.: https://orcid.org/0000-0001-9368-5237

C.P.-C.: https://orcid.org/0000-0001-7728-8936

Abstract

Background and Aims Portable magnetic resonance imaging (MRI) is a promising tool to study water in plant roots, as it is non-invasive and allows measurements outside the laboratory. We aim, using this method, to investigate root structure-function relationships in ten herbaceous species with diverse root traits.

Methods The species were grown in well-watered rhizotrons with the roots separated from the soil. The MR signal from water in the roots was measured using a unilateral MRI to evaluate the water quantity present in the measurement volume, as well as the transverse relaxation time which gives information on water mobility. Ecophysiological and morphological measurements were also performed.

Results A positive relationship was observed between the intensity of the root water MR signal and the root water quantity across species. Diurnal variation in the transverse relaxation time was consistent with changes in leaf water potential and soil humidity. Additionally, the water pool fraction linked to the long transverse relaxation time was negatively related to fine root tissue density, a proxy of stele fraction. In addition, our results indicated the presence of root structure-function relationships in water-use, as illustrated by negative relationships between specific root length and root water quantity derived from MR signal, and between fine root tissue density and water mobility derived from T_2 measurements.

Conclusion This proof-of-concept study demonstrated the capacity of portable MRI to estimate root water quantity and to detect its diurnal fluctuation in various herbaceous species exhibiting diverse water-use strategies.

Keywords

Dicotyledons, Leaf water potential, Monocotyledons, Root traits, Soil humidity, Stomatal conductance

Abbreviations

ΔLWP = Daily variation of leaf water potential

ΔSWC = Daily variation of soil water content

B_0 = Static magnetic field

CPMG = Carr-Purcell-Meiboom-Gill

Gs = Stomatal conductance

ILT = Inverse Laplace transform

LA = Leaf area

LWP = Leaf water potential

MRI = Magnetic resonance imaging

NMR = Nuclear magnetic resonance

NMR-MOUSE = NMR Mobile universal surface explorer

NNLS = Non-negative least square

PCA = Principal component analysis

RF = Radiofrequency

RTD = Root tissue density

RWC = Root water content

SLA = Specific leaf area

SNR = Signal-to-noise ratio

SRL = Specific root length

SWC = Soil water content

T_1 = Longitudinal relaxation time

T_2 = Transverse relaxation time

INTRODUCTION

In plant ecology, the functional approach has revealed a consistent fundamental trade-off between leaf traits linked to resource acquisition and conservation (e.g., Grime et al., 1997; Reich, 2014; Westoby et al., 2002). Some research has indicated that this trade-off can also be applied to root traits (Fort et al., 2017; Prieto et al., 2015; Roumet et al., 2016). However, our understanding of structure-function relationships in plant roots remains limited (Hummel et al., 2007; Wahl and Ryser, 2000; Zhou et al., 2022). Their presence in the intricate soil medium influences the plasticity of root traits, such as diameter, specific root length (SRL), and root tissue density (RTD). Additionally, the spatial arrangement of roots within the same root system, specifically the branching order, significantly alters the trait values (McCormack et al., 2015; Picon-Cochard et al., 2012). At one end of the root economic spectrum, fine root traits, such as a small average root diameter and low RTD, coupled with high SRL, facilitate rapid acquisition strategies by enabling soil exploration for nutrients and water at a fine scale with minimal carbon investment per unit of root length. At the other end, the root economic spectrum is characterized by coarse roots with dense tissues aligning with resource conservation strategies (Fort et al., 2017; Hummel et al., 2007; Picon-Cochard et al., 2012), and exhibiting higher hydraulic conductivity (Masumoto et al., 2022; Rieger and Litvin, 1999; Zhou et al., 2022). Although the root economic spectrum was initially developed for carbon and nitrogen cycling, it is uncertain whether it applies to plant water-use, especially in well-watered conditions. Unraveling the structure-function relationships of plant roots from a water-use perspective would enhance our understanding of their water-use strategies.

Root water-use entails two components, with water being transferred through radial and axial pathways. The radial pathway, which is responsible for water absorption, occurs from the cortex to the stele. The axial pathway, which is responsible for water transport, occurs within the stele and is influenced by transpiration and anatomical traits, such as vessel size and number. Studies have underscored that anatomical features of the roots, including the size of the cortex and stele, reflect both absorption and transport functions (Masumoto et al., 2022; Rieger and Litvin, 1999; Zhou et al., 2022). Nonetheless, the notion of a root economic spectrum for water-use based solely on root diameter has been proven inaccurate. Zhou *et al.* (2021) demonstrated that there was no consistent correlation between root and stele diameters, and that cortex and stele proportions varied across species even when root diameter values were identical. Furthermore, a trade-off between root water uptake and transport was observed not only across root orders but also along a root segment, with changing cortex and stele proportions (Heymans et al., 2021, 2020; Masumoto et al., 2022; Zhou et al., 2022). Although root diameter and RTD might serve

as proxies for root hydraulic conductivity, they do not provide information on vessel size and number (Zhou et al., 2021). Nonetheless, it appears that RTD is a better indicator of root water-use than root diameter, as it has been correlated with stele proportion (Hummel et al., 2007; Masumoto et al., 2022; Wahl and Ryser, 2000), potentially serving as the foundation for a root economic spectrum for water-use. However, measuring this trait requires root destruction, prompting the need for a non-destructive method to estimate it in intact plants.

Imaging techniques have the potential to measure root traits non-destructively. Methods such as visible light imaging, positron emission, neutron and X-ray tomography, and magnetic resonance imaging (MRI) are valuable tools for studying plant structure and/or function. For instance, visible imaging (Doussan et al., 2006), MRI (Pohlmeier et al., 2008), and neutron tomography (Zarebanadkouki et al., 2013) have been used to visualize root system architecture as well as water uptake. Among these imaging methods, MRI has several advantages. It allows for the non-invasive study of water properties by measuring the protons of hydrogen nuclei (^{1}H), without ionizing the sample. and is, therefore, well suited to study the state of water in intact plants. Two relaxation phenomena occur during the recording of the MR signal, each being characterized by a decay rate: the longitudinal relaxation time (T_1) and the transverse relaxation time (T_2).

Depending on the MR acquisition parameters, different contrasts can be chosen, such as proton density, T_1 or T_2 relaxation times (Van As, 2007). Proton density provides information on the amount of water, while relaxation times, particularly the transverse relaxation time T_2, provide information on water mobility and compartmentation. High T_2 values are typically associated with free or mobile water, such as the water within vacuoles or flowing to meet transpiration demand, while low T_2 values indicate water molecules in a restricted state, such as those confined within cell walls (Van As, 2007). Although MR spectrometers are predominantly found in laboratories, low-field instruments with a static magnetic field B_0 of around 1 Tesla or less offer portability, making them ideal for studying plants in their natural environments. This approach has enabled investigations into organ structure and function in varying states of hydration, both within and outside laboratory settings (Blystone et al., 2024). Studies have examined the stem structure (Kimura et al., 2011; Nagata et al., 2016; Terada et al., 2020), fluxes in xylem and phloem tissues (Terada et al., 2020; Windt et al., 2006), seasonal growth patterns of tree stems (Nagata et al., 2016), xylem embolism formation (Meixner et al., 2020), and changes in water content under different hydration conditions (Malone et al., 2016). However, these experiments primarily focused on plant stems, constrained in size by the magnet bore diameter. Other plant organs, such as leaves (Capitani et al., 2009) and roots (Bagnall et

al., 2022, 2020; Nuixe et al., 2021), have also undergone examination. While Bagnall *et al.* (2020, 2022) focused on root detection and imaging in natural soils to understand root morphology, architecture, and development, our study focuses on root structure and function regarding plant ecophysiology and water-use.

In a prior investigation, we demonstrated the suitability of a unilateral and portable device in characterizing root water status across day-and-night cycles in three herbaceous species (Nuixe et al., 2021). The current study aims to go further and determine whether portable, depth-resolved NMR, i.e., 1D-MRI, later referred to as MRI, can elucidate root structure-function relationships in various herbaceous species with diverse root traits. These plants were grown in well-watered rhizotrons to better grasp herbaceous water acquisition strategies. Given that MRI proton density correlates with water quantity, and the T_2 relaxation time provides insights into water mobility and tissue interactions, we hypothesized that (i) MR profiles acquired with the unilateral MRI will allow for root water quantity measurements, and that (ii) variations in T_2 across day and night cycles will correlate with changes in plant water-use dynamics and root traits related to axial water transport, such as RTD.

MATERIALS AND METHODS

Plant material and environment

One *Lupinus angustifolius* (LA), three *Medicago sativa* (Maga variety) (MS), four *Onobrychis viciifolia* (Perly ecotype) (OV), and three *Trifolium pratense* (TP) plants were germinated from seeds. Additionally, one *Plantago lanceolata* (PL), one *Rumex acetosa* (RA), one *Taraxacum officinale* (TO), three *Trifolium repens* (TR) plants, as well as three tillers of *Dactylis glomerata* (DG) and *Festuca arundinacea* (FA) were transplanted from the site of Saint-Genès-Champanelle (France). All plants were grown as monocultures in rhizotrons. The rhizotrons were parallelepiped containers measuring 95 cm in height, 40 cm in length, and 5 cm in width. One side of the container had a transparent wall with a thickness of 4 mm, and the bottom had drainage holes. An 800-g layer of pozzolan was also placed at the bottom for drainage. Nine out of the ten rhizotrons were filled with an upland grassland soil (Cambisol type), which had been sieved to 7 mm and had a pH of approximately 6.5. The soil consisted of 12% clay, 17% silt, 59% sand and 13% organic matter. The remaining rhizotron, intended for *O. viciifolia*, was filled with a mixture of the aforementioned soil and a Limagne soil (Luvisol type) in a 60/40 ratio to increase the pH. Both types of soil were mixed with a slow-release fertilizer to achieve a final concentration of 5 g L^{-1} (NPK 14-7-14, Multicote 12, Haifa, Israel). To separate the root system from the soil while still allowing the transfer of nutrients and water, a nylon polyamide

textile measuring 100 cm in height, 45 cm in length, and 60 µm in width, with a 30-µm mesh and an open surface area of 20% of the pores, was placed between the transparent wall and the soil (Fig. 1.A).

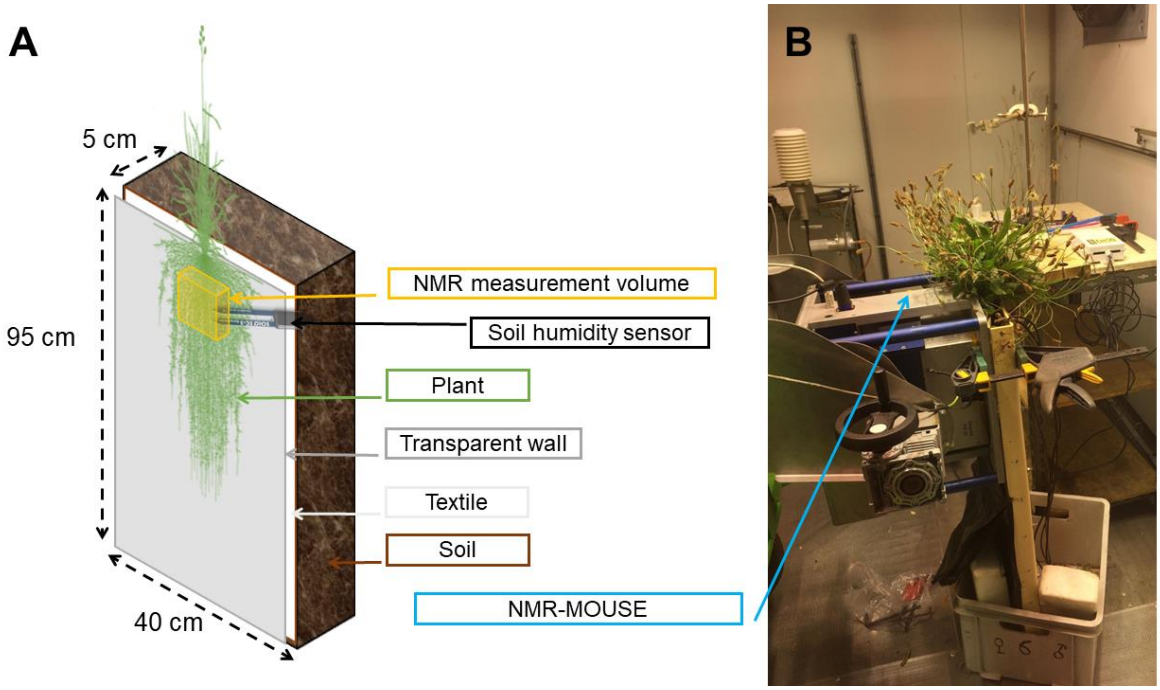

Fig. 1 A. Schematic representation of the rhizotron model. The parallelepiped model was composed of a transparent wall (4 mm thick), the plant roots, and the soil. The textile allowed for the roots to be physically separated from the soil. **B.** The unilateral MRI was positioned against the transparent wall and close to the soil humidity sensor, and measurements were taken through the width of the rhizotron. The MR measurement volume (yellow cube in subset A) was 4 cm × 4 cm × 100 µm.

The rhizotrons containing the plants were left outside during winter 2019 and spring 2020, and the foliage of the plants was cut several times to regenerate it. To minimise the influence of environmental changes on the measurements, the plants were placed in a climatic chamber two to three days before the measurements. This allowed the species to acclimatise to the chamber conditions. A day-and-night cycle was applied in the climatic chamber with lights on from 8 am to 10 pm. The ambient temperature was maintained at 21°C during the day and 18°C at night. Environmental conditions were monitored and recorded at 30s-intervals with a data logger (CR6-Wifi, Campbell Scientific Ltd., Loughborough, UK) and averaged over 5-min periods for CO_2 concentration (CARBOCAP, GMP343, Vaisala, Finland), and with a HOBO data logger (ONSET, Bourne, MA, USA) every ten minutes for relative air humidity and temperature (Supplemental Fig. S1). Ecophysiological and MR measurements were performed on the rhizotrons over a period of one week between July and October 2020 (Supplemental Table S1). All plants, except for *L. angustifolius* which was approximately seven months old, were over one year old at the time of the measurements.

Ecophysiology and traits

Leaf water potential (LWP, in MPa) was measured every fifteen minutes using a psychrometer (PSY1-Stem, ICT International, Armidale, NSW, Australia). The measurements were performed on one, two or three healthy and well-developed leaves, depending on material availability during plant development and the quality of the measurement. Values were then averaged (Supplemental Fig. S2). The mean variation of leaf water potential (ΔLWP) was calculated as the difference between the minimum day LWP and the end-of-night LWP to analyze water consumption. We were unable to obtain LWP measurements for *L. angustifolius* due to the narrowness of its leaves.

Abaxial stomatal conductance (Gs, in mmol m^{-2} s^{-1}) was measured with a porometer (AP4, Delta-T Devices Ltd, Cambridge, UK) on three healthy and well-developed leaves, three times a day: morning, midday and afternoon. Values were then averaged (Supplemental Fig. S2). For the same reason that we were unable to obtain LWP measurements, the Gs of *L. angustifolius* was not recorded.

Soil water content (SWC, in %) was measured every fifteen minutes using a 5-cm long sensor (EC-5, DecagonMeter Group, Pullman, WA, USA) placed horizontally at 16 cm from the top of the rhizotron before plant installation (Supplemental Fig. S3). The sensor was connected to a data logger (EM50, DecagonMeter Group, Pullman, WA, USA). Daily variation of soil water content (ΔSWC) was calculated as the difference between the minimum SWC during the day and the SWC at the end of the night to analyze water consumption. SWC measurements were unsuccessful in the case of *L. angustifolius*.

At the end of the experiments, the rhizotrons were harvested and the plants were cut and sorted by organ type. The total leaf area (LA, in m²) of green leaves was measured using a leaf area meter (Licor 3100, Licor, Lincoln, NE, USA). The specific leaf area (SLA, in cm^2 g^{-1}) was measured on the leaves where the stomatal conductance was recorded. Roots that were present inside the MR measurement window, at approximately 16 cm from the top of the rhizotron, were collected, washed, and frozen in a plastic bag (-18°C) before performing root morphology measurements. After defrosting, the roots were stained with methylene blue dye (5 g L^{-1}) by soaking them for at least 15 minutes at ambient temperature. They were then rinsed with water to remove any excess stain and separated into coarse (>1 mm) and fine roots. The roots were then spread out in a glass tank containing a small amount of water and covered with a transparent film to prevent their dehydration during the scan. Afterwards, they were scanned using a flatbed scanner (EPSON perfection V700; Seiko Epson Corp., Suwa, Japan) in

transparent mode at a resolution of 800 dpi. For each species, 6 to 10 images were recorded and thereafter analyzed using WinRhizoPRO software (V2012b, Régent Instruments, Québec, Canada) to determine root length (in m), average root diameter (RootD, in mm), and root volume (RootV, in cm^3) by diameter class (12 classes, including 10 classes of 0.1 mm-wide increments from 0 mm to 1 mm in diameter, one class for diameters between 1 mm and 2 mm, and one class for diameters higher than 2 mm). To prevent bias resulting from a skewed distribution of root diameters, the root volume was calculated as the sum of each volume by diameter class. Root water quantity (RWQ, in g) was obtained by calculating the difference between fresh mass and dry mass. The dry mass was obtained by oven-drying the fresh roots during 48 hours at 60°C. Root water content (RWC, in g g^{-1}) was calculated as RWQ divided by dry mass. Specific root length (SRL, in m g^{-1}) was calculated as the ratio of length to dry mass (m g^{-1}). Root tissue density (RTD, in g cm^{-3}), measured for all root types, was calculated as the ratio of dry mass to volume. Additionally, RTD was also calculated for fine roots only (< 1mm) and is referred to as FineRTD in the text.

MR experiments

The MR experiments were conducted using a 0.3T PM25 NMR-MOUSE spectrometer (Magritek, Wellington, NZ) with a ^1H resonance frequency of approximately 13.23 MHz. The sensor comprises a permanent magnet, the configuration of which results in a strong gradient of approximately 7.5 T m^{-1} along the B_0-(z)-direction, outwards from the surface of the magnet. Combined with a linear surface coil for radiofrequency (RF) transmission and signal reception, this linear gradient enables selective signal measurement, within a flat sensitive volume with a thickness of 100 µm, at a fixed distance of 25 mm from the magnet surface. In our configuration, a 4 cm by 4 cm surface RF coil was placed on top of a 10-mm thick spacer, which was positioned on top of the magnet, resulting in a distance of 15 mm between the coil and the sensitive volume. Measurements at various depths were achievable due to a high-precision lift that moved both the magnet and the RF coil downwards along the z-direction. The NMR-MOUSE was equipped with a Kea® console (Magritek, Wellington, NZ) and fixed on a positioning device specifically designed to transport the system and to match its position to the desired measurement zone. Here, the surface of the spectrometer was placed in contact with the transparent wall of the rhizotron and clamped to it, centering the measurement zone on the middle of the rhizotrons, at approximately 16 cm from the top of the rhizotron to coincide with the position of the soil humidity sensor (Fig. 1.B).

Profiles, or depth dependent MR signal intensity, were acquired continuously over three consecutive days. The measurement volume was shifted from 14.7 mm (soil in most cases, except for *R. acetosa*) to 0 mm (transparent wall) in increments of 0.1-mm. The signal at each depth, expressed in µV, was acquired using a Carr-Purcell-Meiboom-Gill (CPMG) sequence (Meiboom and Gill, 1958) with the following parameters: 256 echoes, an excitation pulse duration of 15 µs, an echo time of 113 µs, and a repetition time of 3000 ms. The measurements were repeated four times for signal averaging, except for *T. pratense* and *P. lanceolata*, on which the measurements were taken before the protocol was settled and for which eight accumulations were performed. To compare profiles between species, the MR signal of *T. pratense* and *P. lanceolata* was divided by the ratio of the accumulations (8/4), as all other acquisition parameters were identical. For ease of comparison, the signal from the transparent wall was removed from all profiles, and the root zone was set at 0 mm (for visualization of the raw data, please refer to Supplemental Fig. S4). By default, the 256 echoes from the CPMG decay were averaged, leading to a signal that was both proton density and T_2-weighted. To obtain quantitative results, the CPMG decays recorded at all depths assigned to the root compartment were summed to increase the signal-to-noise ratio (SNR). The signal decay was adjusted with a mono and bi-exponential model, and then an F-test and a relative likelihood of bi-exponential test were performed to determine which model best fit our results.

Transverse relaxation time (T_2) measurements were also performed for each species at the depth displaying the maximum of signal in the root zone on the profile. Transverse decay curves were recorded continuously over two consecutive days using a CPMG pulse sequence with the following parameters: 2800 echoes, an excitation pulse duration of 12 µs, an echo time of 100 µs, and a repetition time of 12 s for all species except *P. lanceolata*. For this species, the different acquisition parameters were 2500 echoes, and a repetition time of 10 s. 128 accumulations were performed for *D. glomerata* and *P. lanceolata* and 256 accumulations for the other species. The differences in acquisition parameters arise from the fact that measurements for *D. glomerata* and *P. lanceolata* were taken before the protocol was fully established. The difference in these experimental parameters had no influence on the relaxation analysis (repetition time values were set to the minimal value to respect the RF duty cycle). To investigate the T_2 distribution in each sample, inverse Laplace transforms (ILT) were used to fit our decay curves. The signal decays were first preprocessed by removing the first nine echoes and those following the first negative amplitude value. Assuming that the measured echo decay is a combination of exponential decays, the signal can be expressed as follows:

$$S_i = \sum_{j=1}^{M} A_j e^{-t_i / T_{2j}}, i = 1,2,\ldots,N \quad [1]$$

Where t_i is the measurement time, M is the number of exponential components, N is the total number of echoes, and A_j is the relative amplitude for each partitioned T_2 time, T_{2j}.

ILT analysis was then performed using an in-house Matlab® (MathWorks, Natick, MA, USA) implementation of the non-negative least square (NNLS) inversion algorithm (Whittall and MacKay, 1989). The NNLS algorithm was fed with a large number M, i.e., 150, of T_2 values logarithmically spaced from 3 ms to 1000 ms. The resulting solution was a sparse matrix on which a Tikhonov regularization parameter alpha (Whittall and MacKay, 1989) of between 1.0025 and 1.0030 was applied to control the trade-off between stability and bias. The regularized NNLS solution was then a set of amplitudes A_j and T_{2j} that minimize:

$$\sum_{i=1}^{N} \left| \sum_{j=1}^{M} A_{ij} S_j - y_i \right|^2 + \alpha \sum_{j=1}^{M} \left| S(T_{2j}) \right|^2, \alpha \geq 0 \quad [2]$$

Over 90% of these regularized NNLS fittings provided two T_2 components. For the remaining 10%, when more than two components were obtained, an average of the values of the same order of magnitude was calculated, whereas when only a single value was obtained, a mono-exponential fit was performed on the concerned decay.

Statistical analysis

Correlations and principal component analysis (PCA) were performed to search for and analyze relationships between MR values, morphological, and ecophysiological measurements using R.4.2.1 software (R Core Team, 2022). *L. angustifolius* was excluded from the PCA due to the absence of LWP, SWC and T_2 values. Figures were then produced using the packages ggplot2 and factoextra.

RESULTS

MR profiles

The profiles recorded for each species exhibiting a similar end-of-night leaf water potential (between 0 and -0.38 MPa), and, therefore, operating under similar functioning conditions, are illustrated in Fig. 2. As these profiles were constructed by averaging the amplitudes of the 256 echoes of the CPMG decays at each depth, they gave information on both the water quantity and its relaxation properties, while also allowing insights into the identification of the rhizotron compartments. Notably, the root compartment was discernible by its elevated MR signal

intensities, which varied depending on the species. Across all species, a region of lower MR signal intensities (<0.01 to 0.06 µV) was consistently observed, indicative of the soil compartment, except in the case of *R. acetosa*. For this species, root growth extended beyond the inner space delimited by the plexiglass and the textile, exceeding the 15 mm observation limit.

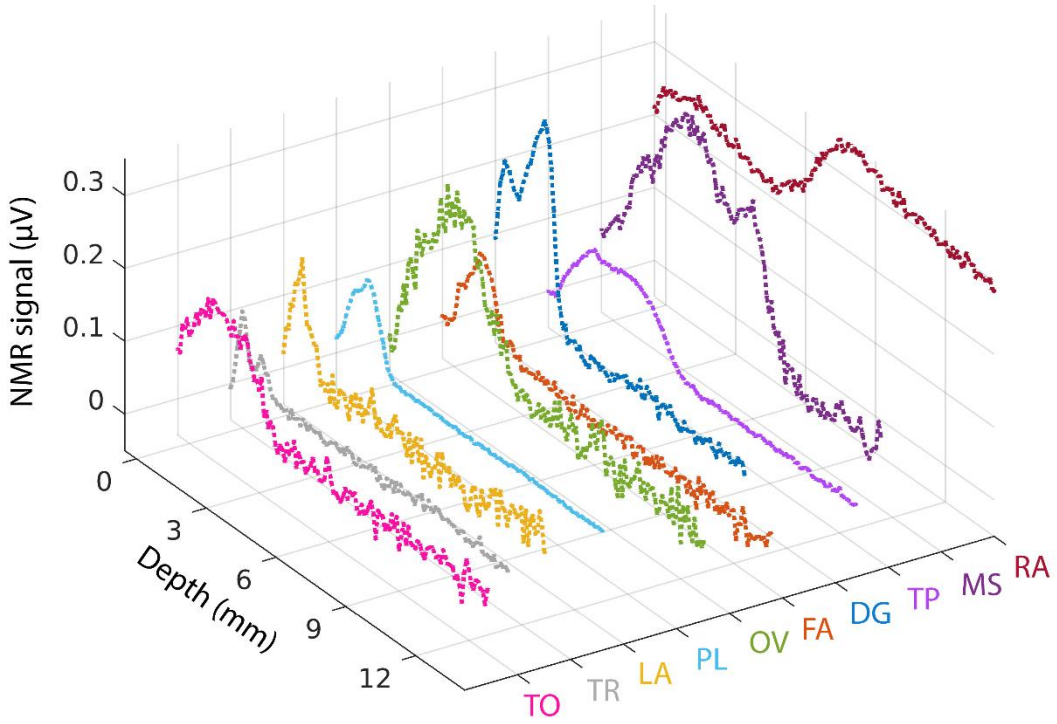

Fig. 1 MR profiles (MR signal intensity in function of the measurement depth) of *T. officinale* (TO), *T. repens* (TR), *L. angustifolius* (LA), *P. lanceolata* (PL), *O. viciifolia* (OV), *F. arundinacea* (FA), *D. glomerata* (DG), *T. pratense* (TP), *M. sativa* (MS) and *R. acetosa* (RA) acquired through the width of the rhizotron, at equivalent end-of-night LWP, between 0 and -0.38 MPa. The high signal amplitude region corresponded to the roots, while the low signal amplitude region corresponded to the soil.

The profiles were contrasted among species in signal intensity, with the root region peaks of *T. pratense*, *T. repens, F. arundinacea* and *P. lanceolata* barely reaching 0.1 µV, while those of *R. acetosa* were consistently near 0.3 µV. The profiles also differed in the width of the root region, which ranged from 1.6 mm for *L. angustifolius* and *T. repens* to 14.7 mm for *R. acetosa*. Some profiles exhibited an inflection point that divided the root region into two peaks. The inflection point was located at 1.1 mm for *T. repens* and *D. glomerata*, 2.4 mm for *T. pratense*, 5.5 mm for *M. sativa* and 5.4 mm for *R. acetosa* (Fig. 2).

Leaf and root morphological and ecophysiological traits

Table 1 summarizes the leaf and root morphological and ecophysiological traits. The leaf area varied from 0.01 m² for *L. angustifolius* to 0.62 m² for *T. officinale*. The specific leaf area and

stomatal conductance showed a positive co-variation, with a 2.5-fold change for SLA and a 9.2-fold change for Gs between species. Leaf water potential differences between night and day (ΔLWP) showed contrasting water-use between plants for which the difference was low (*R. acetosa*, *F. arundinacea* and *O. viciifolia)* and plants in which this difference was high (*D. glomerata*, *T. officinale*, *T. repens* and *M. sativa*). The variation of SWC (ΔSWC) was contained for all species (< 4%). The time evolutions of LWP and SWC are presented on Supplemental Fig. 2 and 3, respectively. Highly contrasting root characteristic values were observed among the species within the measured volume. Root volume (RootV) and root tissue density showed a positive correlation. Species with low RootV exhibited low RTD (*T. officinale, L. angustifolius*, *P. lanceolata*), while those with high RootV showed high RTD values (e.g., *R. acetosa*, *M. sativa).* Additionally, as expected, a negative relationship was observed between root diameter and SRL. Species with low diameter had high SRL values (e.g., *T. officinale*, *F. arundinacea*, *P. lanceolata*), whereas species with high diameter had low SRL values (e.g., *O. viciifolia*, *R. acetosa*, *L. angustifolius*).

Table 1 Leaf and root morphological and ecophysiological traits measured on the 10 species. The symbol "—" indicates missing data.

Species	LA (m^2)	SLA ($cm^2\ g^{-1}$)	Gs (mmol $m^{-2}\ s^{-1}$)	ΔLWP (MPa)	ΔSWC (%)	Root V (cm^3)	Root D (mm)	SRL ($m\ g^{-1}$)	RTD ($g\ cm^{-3}$)	FineRTD ($g\ cm^{-3}$)	Root M (g)	RWC ($g\ g^{-1}$)	RWQ (g)
***T. officinale* (TO)**	0.62	232.57	952.78	-1.48	-3.80	0.08	0.16	277.2	0.157	0.157	0.01	0.83	0.01
***T. repens* (TR)**	0.24	147.12	366.57	-1.39	-2.05	0.15	0.22	98.0	0.263	0.259	0.04	0.73	0.03
***L. angustifolius* (LA)**	0.013	91.73	—	—	—	0.38	0.51	54.4	0.061	0.061	0.02	0.85	0.02
***P. lanceolata* (PL)**	0.22	183.45	444.07	-0.93	-1.79	0.78	0.27	202.8	0.176	0.136	0.13	0.81	0.11
***O. viciifolia* (OV)**	0.54	104.39	122.55	-0.53	-0.40	1.46	0.76	50.6	0.234	0.177	0.31	0.79	0.25
***F. arundinacea* (FA)**	0.17	145.66	199.13	-0.41	-2.51	2.10	0.23	158.3	0.160	0.198	0.35	0.77	0.27
***D. glomerata* (DG)**	0.61	107.66	104.10	-1.82	-2.51	2.43	0.22	133.2	0.203	0.220	0.51	0.77	0.39
***T. pratense* (TP)**	0.22	192.30	—	-0.81	-0.83	3.11	0.30	108.4	0.217	0.182	0.69	0.79	0.54
***M. sativa* (MS)**	0.5	163.34	—	-1.09	-1.83	5.65	0.43	105.1	0.292	0.212	1.63	0.68	1.10
***R. acetosa* (RA)**	0.36	207.47	396.49	-0.36	-0.99	18.27	0.66	53.5	0.275	0.174	4.96	0.65	3.22

Fig. 3 presents a detailed analysis of root volume, illustrating the proportion of different root diameters. The results indicate that *R. acetosa*, *M. sativa* and *T. pratense* had 94%, 77% and 58% of their root volume, respectively, comprised of coarse roots, i.e., roots having a diameter greater than 1 mm. In contrast, 67%, 55% and 53% of the root volume of *T. officinale*, *P. lanceolata* and *T. repens*, respectively, consisted of very fine roots, i.e., with a diameter lower than 0.4 mm. The two monocots had root diameters no greater than 2 mm, with their root volumes evenly distributed across all diameters.

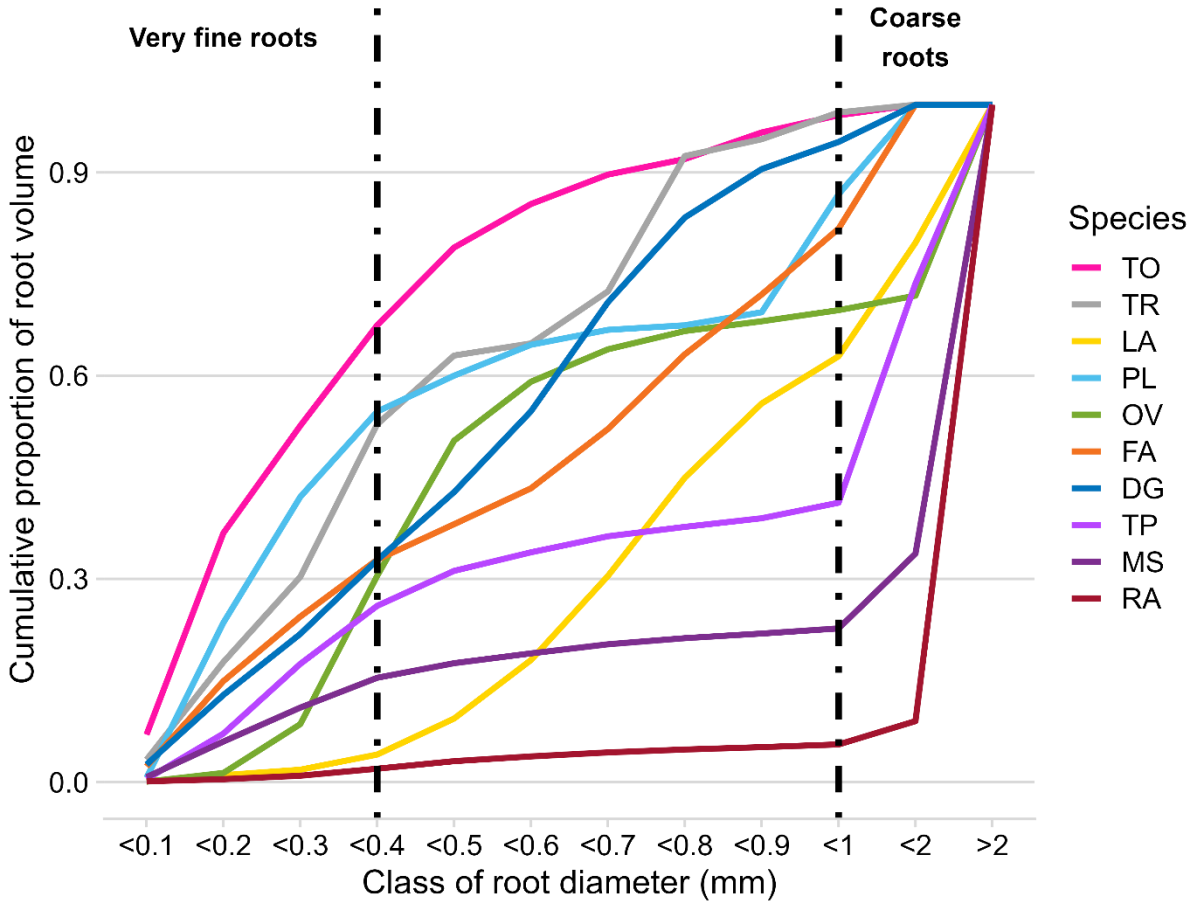

Fig. 3 The cumulative proportion of root volume per class of root diameter (mm) measured within the MR measurement zone for each species. Coarse roots were defined as roots with a diameter higher than 1 mm, while very fine roots were defined as roots with a diameter lower than 0.4 mm.

Links between root morphological traits, ecophysiological traits, and MR profiles

The quantitative information pertaining to the depth profiling was obtained by taking the initial amplitude of the fit of the signal decay, averaged over 256 echoes, within the root compartment. The best model for all species on the root signal was a model containing two proton pools. The sum of the amplitudes of the short T_2 and long T_2 pools, denoted $AT_{2,profile}$ later in the text, correlated positively with the root water quantity (r^2= 0.97, p-value<0.05, Fig. 4).

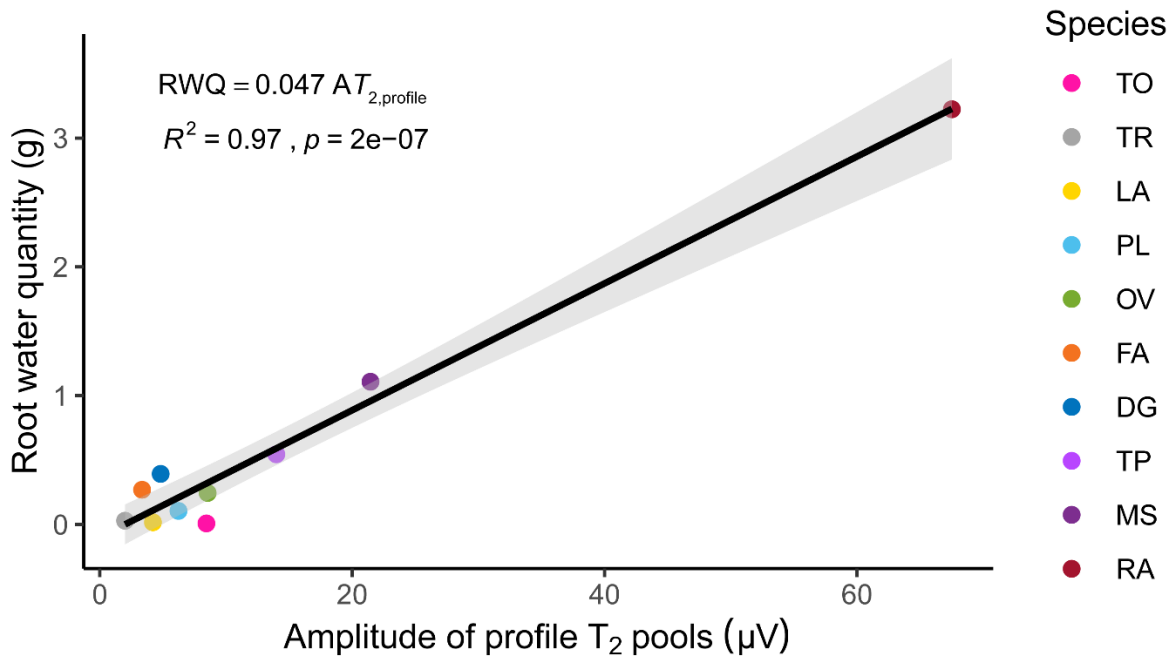

Fig. 4 Linear relationship observed between the root water quantity and the sum of the amplitude of T_2 pools ($AT_{2,profile}$).

Temporal evolution of the transverse relaxation times (T_2) measured in roots

Fig. 5.A shows the temporal evolution of the values of the short and long transverse relaxation times measured at the depth displaying the maximum signal intensity for each species. Apart from *L. angustifolius*, for which the signal intensity was insufficient for analysis, the measured short T_2 value displayed moderate intra- and inter-species changes for the other nine species, with a mean value of around 5.0 ms. Conversely, higher amplitude variation was observed for the long T_2 value between species. Indeed, at night, the long T_2 value varied between a mean value of 29.9 ms for *F. arundinacea* and 75.9 ms for *P. lanceolata*. During the day, the mean long T_2 value ranged from 31.7 ms for *F. arundinacea* to 66.0 ms for *O. viciifolia*. Globally, four species, i.e., *T. officinale*, *D. glomerata*, *O. viciifolia*, and *P. lanceolata*, had mean long T_2 values greater than 50 ms. A day-night variation of the long T_2 value was present in three out of nine species, namely, *O. viciifolia*, *D. glomerata*, and *P. lanceolata*. For these species, the value of the T_2 at night was systematically higher than the value of the T_2 during the day ($T_{2,day}$). The increase ranged from 7.3% for *O. viciifolia* to 15.7% for *P. lanceolata*. While the proportion of the two water pools characterized by short and long T_2, respectively, did not vary significantly between day and night for each species, these fractions varied greatly between species (Fig. 5.B).

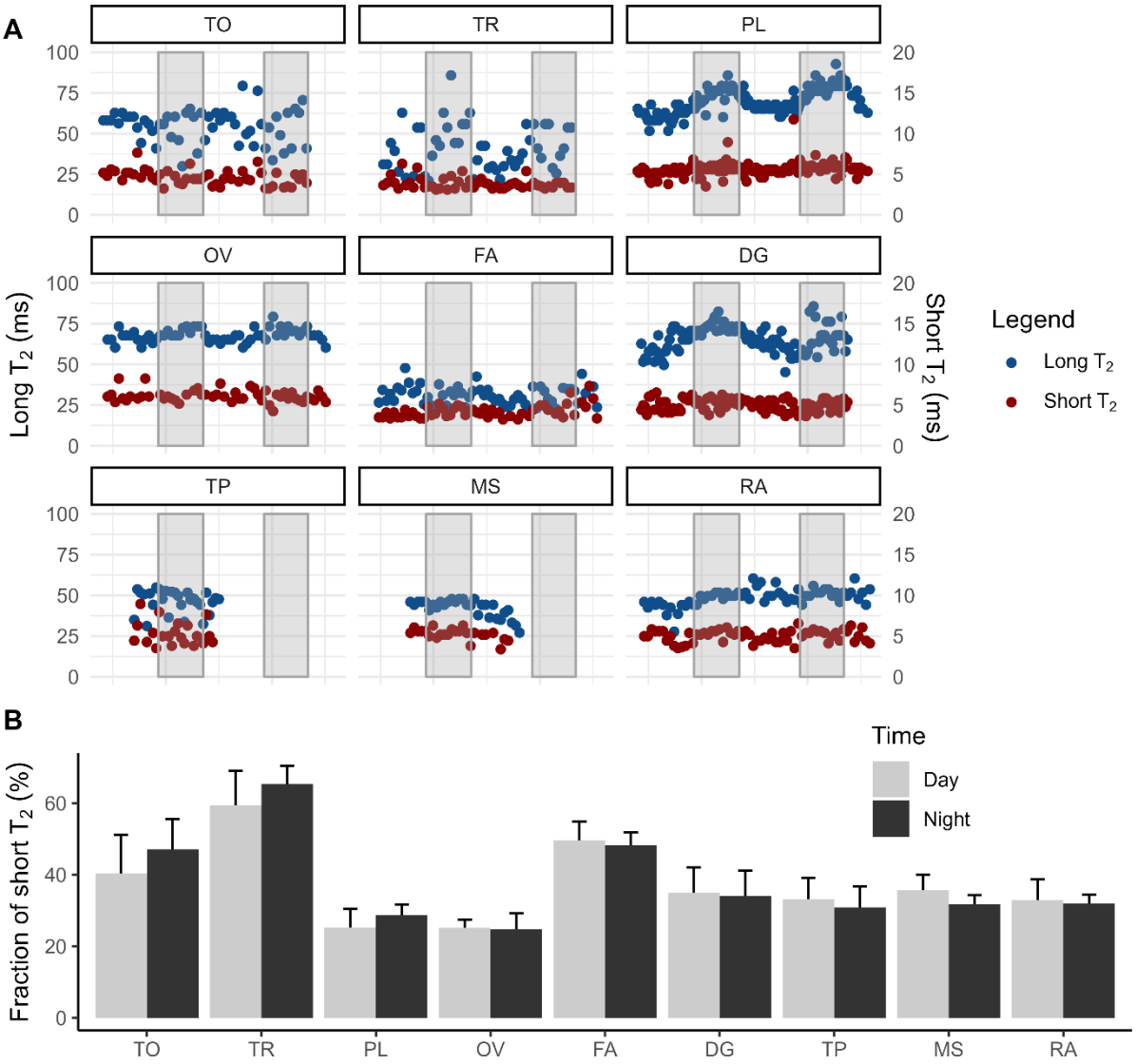

Fig. 5 A. Temporal evolution of short (red) and long (blue) T_2 values for all species measured at one specific depth. The alternation of white and grey rectangles represents the day and night cycle. **B.** Mean and standard deviation of the fraction of the short T_2 pool at night (dark grey) and during the day (light grey) for each species.

Links between root morphological, ecophysiological traits, and T_2 results

A principal component analysis (PCA) was performed to investigate relationships between some root traits, daily variation of leaf water potential, and MR measurements (Fig. 6). 75.3% of the total variance was explained by the two first components. Component 1 was mainly represented by SRL, RWC, RootV, RTD, and $AT_{2,profile}$. Component 2 was mostly represented by the proportion of long $T_{2,day}$ pool (Prop$LongT_{2,day}$) and FineRTD. *T. officinale*, *M. sativa* and *R. acetosa* were well represented on the first axis, while *T. repens* and *P. lanceolata* were best represented on the second axis. In contrast, the two monocots, *O. viciifolia* and *T. pratense* were

poorly represented on these two axes. All numerical PCA results are summarized in Supplemental Table 2.

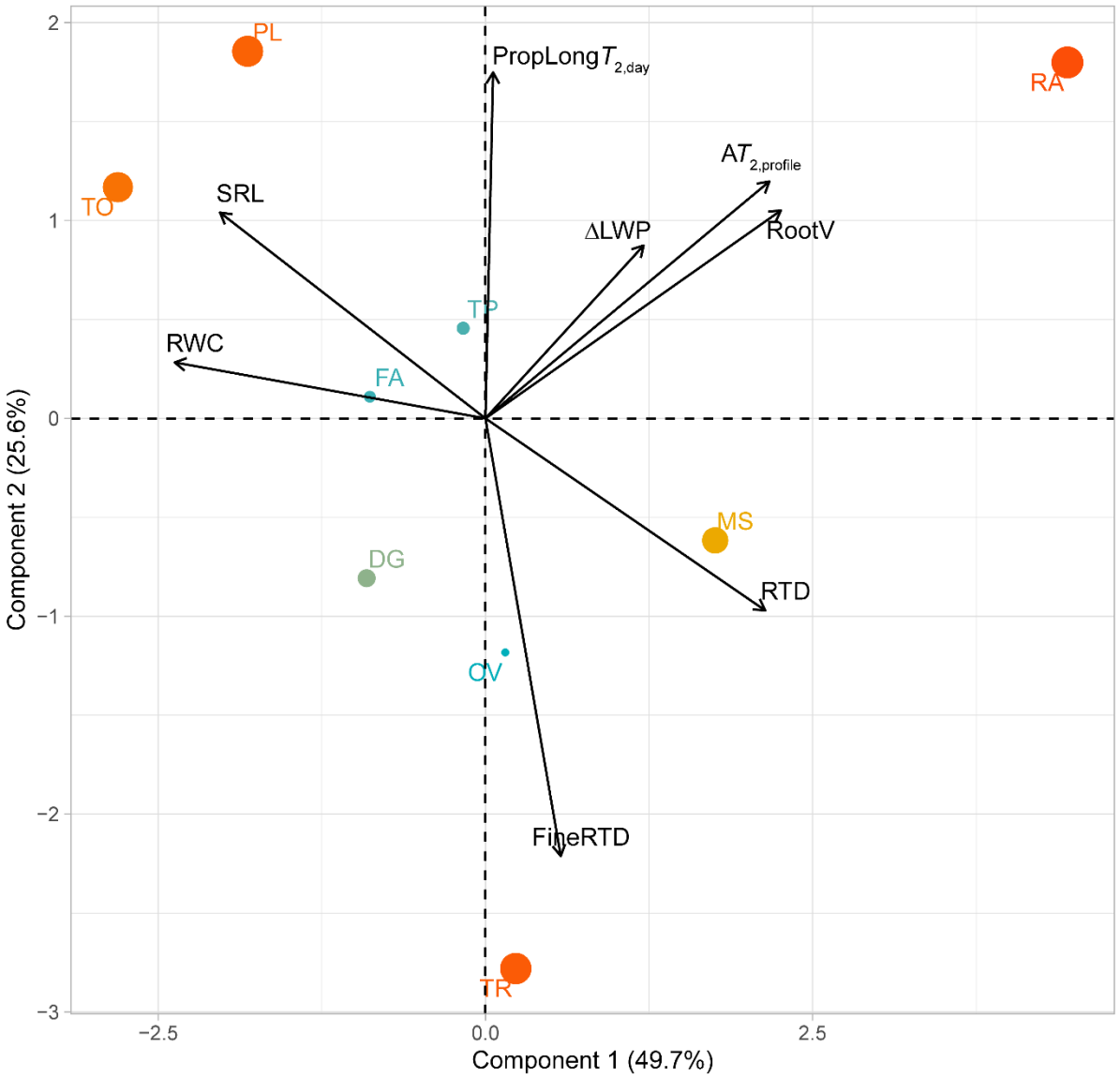

Fig. 6 Two first components of the principal component analysis (PCA) performed with root traits (SRL, RWC, RootV, RTD and FineRTD), ecophysiological (ΔLWP) and MR values ($AT_{2,profile}$ and PropLong$T_{2,day}$). Colors and point size represent the quality of the representation of individuals on the axes; the redder and bigger the point is, the better the species is represented.

DISCUSSION

Nondestructive and quantitative measurements of water can be achieved using MR sensors. In our study, we aimed to determine whether portable MRI can investigate root structure-function relationships in various herbaceous species with diverse root traits grown in rhizotrons. The rhizotron model allowed us to accurately monitor the root water MR signal evolution at a specific position near the soil water sensor, thereby avoiding the contribution of soil water to

the signal. This approach facilitated an evaluation of the potential utility of unilateral MRI for investigating root water status.

Transverse relaxation time T_2 separates the different water pools

The specificity of our MRI sensor is to systematically record the signal using a CPMG pulse train, thereby enabling the measurement of the transverse relaxation time T_2. In this study, depending on whether the objective was to probe the whole profile or to focus on a specific depth, the CPMG acquisition parameters and data processing differed to reach either an appropriate experimental time or signal-to-noise ratio, respectively. However, both approaches led to the same results, i.e., a signal decay containing two water pools with distinct T_2 relaxation times. For each of these pools, the value of the relaxation time, as well as its amplitude, either absolute or relative, was extracted.

T_2 relaxation times in water are influenced by interactions with the surrounding environment. Water molecules that are bound to macromolecules or surfaces have shorter relaxation times than free water molecules (Van As, 2007). In their analysis of the T_2 relaxation times of water in leaves, Musse *et al.* (2017) found a short T_2 value of approximately 3 ms, which they assigned to the water pool bound to macromolecules and cell walls. Similarly, Jones *et al.* (2012) assigned similar T_2 values in wood to bound water. Therefore, we attributed short T_2 values to all the tissue-bound water, regardless of the tissue type, while long T_2 values were assigned to free and/or mobilizable water, i.e., water present within the vacuole of plant cells and/or water present within the xylem in the stele.

MR profiles reveal the root water quantity of ten herbaceous species in a non-destructive way

Here, the MRI detected the whole water signal within its sensitive zone, which was a 4 cm by 4 cm by 100 µm thick parallelepiped. The signal was then a combination of all the roots present within the measurement window, e.g., a mix of fine and coarse roots. The information obtained from the portable MRI was then related to the entire measurement window, rendering it impossible to correlate the results to a single root.

The MR profiles presented in Fig. 2 were constructed by averaging the signal from the 256 echoes of the MR decay acquired at each depth, resulting in profiles weighted in both proton density and transverse relaxation times. This weighting allowed for a clear differentiation between the water in the soil and in the root compartments. The observed contrast was due to differences in water content, i.e., proton density, as indicated by the differences between RWC

and SWC (Table 1 and Supplemental Fig. 3), and in T_2 values. Indeed, the soil is a heterogeneous medium, characterized by a multitude of factors, including texture, porosity, the presence of paramagnetic ions, and so forth. When coupled with the strong magnetic field gradient of the spectrometer, a significant reduction (T_2* effect) in the water T_2 values is observed (Bagnall et al., 2020; Gruwel, 2014; Pflugfelder et al., 2017). For instance, Bagnall *et al.* (2020) reported a minimum factor of 21 between the T_2 of water in roots (from 85 to 140 ms) and the T_2 of water in soil (from 0.33 to 4.14 ms).

Some species exhibited an inflection point on their profile reflecting a variation of the hydric status in the spatial dimension (Fig. 2). One possible explanation is that the roots present in the MRI window have different ages, with younger roots having generally higher RWC than older ones. This is because younger roots are actively growing and conducting water and nutrients, requiring high water content to support their metabolic activities. As roots age and become more lignified, their water content decreases (Freschet et al., 2021). For evenly distributed roots exhibiting a high water consumption (high ΔLWP and ΔSWC values) such as *D. glomerata* (Table 1), this bimodal distribution could also be due to a non-linear water gradient in the roots from the textile (high water content) to the transparent wall (low water content), intensified by the species' water consumption. For species presenting a heterogeneous spatial arrangement of fine and coarse roots in the MRI window like *T. pratense* and *M. sativa* (Supplemental Fig. S5 F and G), the bimodal signal intensity distribution is most likely related to the root density with an intrinsically higher water content where there is a higher root density. Nonetheless, as it was not possible to record 3D images to validate this hypothesis, 3D methods such as high-field MRI (Gruwel, 2014) or X-ray tomography (Mooney et al., 2012) should be considered.

To obtain quantitative data from these profiles, it was critical to remove the T_2-weigthing of our data and to quantify the water content over the whole measurement depth. When measuring the root traits, we measured the water contained in all root tissues. Therefore, the sum of both T_2 relaxation time pools was used to correlate with the water quantity. Despite a good linear relationship obtained ($r^2 = 0.97$), values measured for species with an RWQ below 0.1 g were aggregated as an uncorrelated point cloud, perhaps suggesting that the limit of sensitivity of the NMR-MOUSE had been reached. Therefore, to improve the accuracy of the relationship, additional species with root systems of intermediate and high-water content should be included, as only three species, *T. pratense*, *M. sativa* and *R. acetosa*, were studied from these categories. The Groot database (Guerrero-Ramírez et al., 2021) provides, among other measurements, the root stele fraction for eight out of ten of our species, with the exception of *L. angustifolius* and *T. officinale*. Using this database, it appeared that the root stele fraction was positively related

to our RTD of fine roots (r^2 = 0.67, p-value = 0.014, Supplemental Fig. S6), in agreement with a previous study (Hummel et al., 2007). Among the species studied, *R. acetosa*, *O. viciifolia* and *T. pratense* had a low root stele fraction and/or FineRTD with the highest water quantity as measured by MR, suggesting an inverse relationship between signal amplitude and root stele fraction and/or FineRTD. With regard to *L. angustifolius*, we measured a low FineRTD and thus expected a high MR signal. However, the MR signal was low. This was attributed to the small number of roots present in the measurement zone.

Transverse relaxation times give information on the root function

The short T_2 relaxation time pool was assigned to tissue-bound water. Given that neither its time nor its population fraction exhibited any variation over the two-day experiment period for each species, we concluded that the plants were well-hydrated. Indeed, when plants undergo leaf dehydration during the day, their cells may lose their turgidity due to a reduction in vacuolar volume. This loss can be visible in the decrease in end-of-night LWP which, due to the soil-plant-atmosphere continuum, allows for the estimation of the water potential between the soil and the roots. Compared to other cellular components, the vacuole is characterized by a long T_2 relaxation time (Van As, 2007). Therefore, a reduction in vacuolar volume in water-stressed plants would lead to an increase in the short T_2 fraction, as the long T_2 fraction would decrease. Contrary to short T_2 values, long T_2 values varied between approximately 30 and 76 ms across species, with a clear day-and-night cycle for *P. lanceolata*, *T. repens*, *O. viciifolia* and *D. glomerata*. These values were comparable to those reported in the literature on trees (long T_2 in sapwood and heartwood, Jones *et al.* 2012; stem tissues, Meixner *et al.* 2021) and in the cortex and stele of carrot taproot (Sibgatullin et al., 2010), as well as in vacuoles in leaves (Musse et al., 2013). Based on the literature, and in the absence of sufficient resolution, we could not distinguish water within the vacuole from water transported within the xylem in the stele. The long T_2 times should then be interpreted as an average T_2 encompassing both the cortex and stele (xylem) long T_2 values. Species with long T_2 values shorter than 50 ms, particularly *R. acetosa*, *M. sativa* and *T. pratense*, were among those having a significant proportion of coarse roots and a high RTD, between 0.19 and 0.24. As RTD and root stele fraction have been positively correlated (Hummel et al., 2007; Masumoto et al., 2022; Wahl and Ryser, 2000), and given the greater density of stele tissue in comparison to cortex tissue, as well as the influence of the surrounding environment on T_2 values, our results suggest that lower long T_2 values were associated with denser tissues. Long T_2 pool values could therefore provide insight into the stele fraction, with a lower value indicating a higher root stele fraction. Although this was not done

in the present study, T_2 maps and histological measurements should be considered on single excised roots of different diameters, RTD, and species to confirm the assumption that long T_2 may be a proxy for root stele fraction.

A diurnal variation in long T_2 values with a decrease during the day was observed for several species, including *O. viciifolia*, *P. lanceolata* and *D. glomerata* (Fig. 5.A). T_2 relaxation may be affected by various mechanisms, including changes in magnetic susceptibility due to the presence of paramagnetic particles or air pockets, for instance, or incoherent (diffusion) (Carr and Purcell, 1954) or coherent (flow) (Hemminga et al., 1977) motion, as well as surface-to-volume ratio (Brownstein and Tarr, 1979; Washburn, 2014). Given that each species was monitored at the same position over two consecutive days, it is unlikely that mechanisms, such as the presence of air pockets, would exhibit significant diurnal changes that could alter T_2 to the extent that was observed. Furthermore, the experiments were conducted on well-watered plants, as indicated by the high end-of-night LWP values (between -0.4 and -0.1 MPa for *O. viciifolia*, *P. lanceolata* and *D. glomerata*). Therefore, it is unlikely that the species exhibiting these long T_2 diurnal variations would have experienced significant changes in root size, as can occur when subjected to hydric stress, leading to root shrinkage (Bingham, 2007; Carminati et al., 2009). Finally, the NMR-MOUSE has a natural B_0 gradient that exacerbates the effects of water motion (diffusion and/or flow) along this B_0 direction on the signal, leading to an acceleration of the signal decay and then a decrease of the apparent T_2. Here, because the systematic decrease in the long T_2 value during the day was not observed for all species despite them experiencing the same changes in climatic chamber conditions, we considered the influence of water diffusion to be weak. The decrease in T_2 relaxation times during the day was then mainly attributed to the coherent motions that were involved in plant transpiration. The effect of this motion on the T_2 value can be exacerbated by the sensor B_0 gradient, and the fact that roots grew clearly with a preferential direction (top to bottom) but with a tortuosity, leading to an increase sensitivity to the flow, further impacting the relaxation measurement due to the B_0 gradient. *T. officinale*, *F. arundinacea*, *T. pratense*, *M. sativa* and *R. acetosa* did not exhibit a noticeable diurnal variation in their long T_2. This can be attributed to the fact that the T_2 time is influenced by the fraction of cortex and stele, as previously discussed. Denser tissues are typically associated with a higher root stele fraction and a low relaxation time. However, the stele fraction alone does not provide information on the number of vessels within the stele. Therefore, it is possible that for these species, a low proportion of water flowing in the stele resulted in less sensitive measurements and the inability to observe a diurnal cycle. Further studies are required to investigate this hypothesis.

Traits relationships to define plant water-use

The principal component analysis showed water-use patterns among various, albeit limited, well-watered herbaceous species using trait syndromes. The first principal component axis suggested similarities with regard to the plant economic spectrum, showcasing the anticipated trade-off between resource acquisition and conservation strategies (Moreno-Gutiérrez et al., 2012; Roumet et al., 2016). Specifically, SRL and root water content (negative part), and root volume, global RTD and $AT_{2,profile}$ (positive part) were the major contributors to this axis. *P. lanceolata* and *T. officinale* were found to adopt an acquisitive resource strategy in agreement with previous literature (Molina-Montenegro et al., 2018; Pol et al., 2021), while *R. acetosa* and *M. sativa* leaned towards a conservative strategy. Despite exhibiting conservative characteristics, *M. sativa* exhibited higher values for leaf area, SRL, ΔLWP and ΔSWC compared to *R. acetosa* (Table 1). Furthermore, mean long T_2 values during transpiration hours were lower for *M. sativa* than for *R. acetosa*, indicating a faster water consumption for *M. sativa*, as emphasized by ΔLWP and ΔSWC (Table 1).

The second principal component reflected an axis of water transport capacity, where the proportion of the daily long transverse relaxation time and RTD of fine roots exhibited a negative correlation. The proportion of long T_2 pool provided insights into the availability of free and/or mobilizable water. Our findings aligned with previous research as higher RTD values correspond to a greater proportion of conductive stele within the root tissues (Hummel et al., 2007; Wahl and Ryser, 2000). Since the stele, being denser than the cortex, was associated with a low proportion of long T_2 values (and consequently a high proportion of short T_2), it appeared that the long transverse relaxation time components (value and proportion) were inversely related to stele fraction. As ΔLWP, indicative of transpiration, and long transverse relaxation times are linked with water mobility, we could have expected a correlation between these variables. The lack of direct correlations between them might be attributed to measurement asynchrony and uncertainty about the knowledge of a direct link between the roots and the leaves measured. Nevertheless, both *T. repens* and *P. lanceolata* were well positioned on this second major axis, albeit on opposite sides. *T. repens* was characterized by a higher RTD, a lower value and proportion of long $T_{2,day}$ and a greater disparity in water potential and soil water content compared to *P. lanceolata*, indicating *T. repens* as a species with a higher transpiration rate. This finding was consistent with existing literature, as *T. repens* is known to exhibit poor water regulation through stomatal closure (Lucero et al., 2000) and is sensitive to drought (Signarbieux and Feller, 2012). However, it is important to note that the patterns of

traits relationships revealed by the PCA only apply to the individuals that were studied. Our results cannot be extrapolated to be species-specific due to the lack of both replicates in the individuals and representativity of the entire root architecture, i.e., a single position was studied near the humidity sensor.

In conclusion, our proof-of-concept study demonstrated the capability of portable MRI to estimate root water quantity and detect diurnal fluctuation in various herbaceous species exhibiting diverse water-use strategies. Our findings revealed a negative correlation between root long T_2 components and fine RTD, offering possible insights into root structure, given the association of RTD with the proportion of stele within the roots. Future investigations should explore MRI measurements at different positions within the root system, as root traits vary spatially, and replicate measurements in different rhizotrons for a given species. Additionally, single root measurements should be performed to substantiate certain hypotheses, such as the impact of tortuosity and root intertwining on T_2 results. More complex conditions, incorporating soil-root mixtures and conducting measurements in the field rather than in controlled laboratory environments should also be considered. Such endeavours will contribute to a deeper understanding of plant-water dynamics and root functioning across diverse environmental contexts.

Acknowledgments

We would like to thank David Colosse, Patrick Pichon and Alexandre Salcedo for taking care of the plants. We are also grateful to Abdlatif Benmoussa for his technical support and assistance with the portable MRI and Robert Falcimagne for his help with the climatic chamber.

REFERENCES

Bagnall, G.C., Altobelli, S.A., Conradi, M.S., Fabich, H.T., Fukushima, E., Koonjoo, N., et al. (2022) Design and demonstration of a low-field magnetic resonance imaging rhizotron for in-field imaging of energy sorghum roots. *The Plant Phenome Journal*. 5: e20038.

Bagnall, G.C., Koonjoo, N., Altobelli, S.A., Conradi, M.S., Fukushima, E., Kuethe, D.O., et al. (2020) Low-field magnetic resonance imaging of roots in intact clayey and silty soils. *Geoderma*. 370: 114356.

Bingham, I.J. (2007) Quantifying the presence and absence of turgor for the spatial characterization of cortical senescence in roots of Triticum aestivum (Poaceae). *American Journal of Botany*. 94: 2054–2058.

Blystone, S., Nuixe, M., Traoré, A.S., Cochard, H., Picon-Cochard, C., and Pagés, G. (2024) Towards portable MRI in the plant sciences. *Plant Methods*. 20: 31.

Brownstein, K.R., and Tarr, C.E. (1979) Importance of classical diffusion in NMR studies of water in biological cells. *Phys Rev A*. 19: 2446–2453.

Capitani, D., Brilli, F., Mannina, L., Proietti, N., and Loreto, F. (2009) In Situ Investigation of Leaf Water Status by Portable Unilateral Nuclear Magnetic Resonance. *Plant Physiol*. 149: 1638–1647.

Carminati, A., Vetterlein, D., Weller, U., Vogel, H.-J., and Oswald, S.E. (2009) When Roots Lose Contact. *Vadose Zone Journal*. 8: 805–809.

Carr, H.Y., and Purcell, E.M. (1954) Effects of Diffusion on Free Precession in Nuclear Magnetic Resonance Experiments. *Phys Rev*. 94: 630–638.

Doussan, C., Pierret, A., and Garrigues, E. (2006) Water uptake by plant roots: II – Modelling of water transfer in the soil root-system with explicit account of flow within the root system – Comparison with experiments. *Plant and Soil*. 283: 99–117.

Fort, F., Volaire, F., Guilioni, L., Barkaoui, K., Navas, M.-L., and Roumet, C. (2017) Root traits are related to plant water-use among rangeland Mediterranean species. *Functional Ecology*. 31: 1700–1709.

Freschet, G.T., Pagès, L., Iversen, C.M., Comas, L.H., Rewald, B., Roumet, C., et al. (2021) A starting guide to root ecology: strengthening ecological concepts and standardising root classification, sampling, processing and trait measurements. *New Phytologist*. 232: 973–1122.

Grime, J.P., Thompson, K., Hunt, R., Hodgson, J.G., Cornelissen, J.H.C., Rorison, I.H., et al. (1997) Integrated Screening Validates Primary Axes of Specialisation in Plants. *Oikos*. 79: 259.

Gruwel, M.L.H. (2014) In Situ Magnetic Resonance Imaging of Plant Roots. *Vadose Zone Journal*. 13: 1–8.

Guerrero-Ramírez, N.R., Mommer, L., Freschet, G.T., Iversen, C.M., McCormack, M.L., Kattge, J., et al. (2021) Global root traits (GRooT) database. *Global Ecol Biogeogr*. 30: 25–37.

Hemminga, M.A., de Jager, P.A., and Sonneveld, A. (1977) The study of flow by pulsed nuclear magnetic resonance. I. Measurement of flow rates in the presence of a stationary phase using a difference method. *Journal of Magnetic Resonance (1969)*. 27: 359–370.

Heymans, A., Couvreur, V., LaRue, T., Paez-Garcia, A., and Lobet, G. (2020) GRANAR, a Computational Tool to Better Understand the Functional Importance of Monocotyledon Root Anatomy. *Plant Physiol*. 182: 707–720.

Heymans, A., Couvreur, V., and Lobet, G. (2021) Combining cross-section images and modeling tools to create high-resolution root system hydraulic atlases in Zea mays. *Plant Direct*. 5: e00290.

Hummel, I., Vile, D., Violle, C., Devaux, J., Ricci, B., Blanchard, A., et al. (2007) Relating root structure and anatomy to whole-plant functioning in 14 herbaceous Mediterranean species. *New Phytologist*. 173: 313–321.

Jones, M., Aptaker, P.S., Cox, J., Gardiner, B.A., and McDonald, P.J. (2012) A transportable magnetic resonance imaging system for in situ measurements of living trees: The Tree Hugger. *Journal of Magnetic Resonance*. 218: 133–140.

Kimura, T., Geya, Y., Terada, Y., Kose, K., Haishi, T., Gemma, H., et al. (2011) Development of a mobile magnetic resonance imaging system for outdoor tree measurements. *Review of Scientific Instruments*. 82: 053704.

Lucero, D.W., Grieu, P., and Guckert, A. (2000) Water deficit and plant competition effects on growth and water-use efficiency of white clover (Trifolium repens, L.) and ryegrass (Lolium perenne, L.). *Plant and Soil*. 227: 1–15.

Malone, M.W., Yoder, J., Hunter, J.F., Espy, M.A., Dickman, L.T., Nelson, R.O., et al. (2016) In vivo Observation of Tree Drought Response with Low-Field NMR and Neutron Imaging. *Front Plant Sci*. 7.

Masumoto, T., Ito, T., Akatsuki, M., and Makita, N. (2022) Fine root hydraulic conductivity relates to root functional traits in four coniferous species. *Rhizosphere*. 21: 100489.
McCormack, M.L., Dickie, I.A., Eissenstat, D.M., Fahey, T.J., Fernandez, C.W., Guo, D., et al. (2015) Redefining fine roots improves understanding of below-ground contributions to terrestrial biosphere processes. *New Phytologist*. 207: 505–518.
Meiboom, S., and Gill, D. (1958) Modified Spin-Echo Method for Measuring Nuclear Relaxation Times. *Review of Scientific Instruments*. 29: 688–691.
Meixner, M., Kochs, J., Foerst, P., and Windt, C.W. (2021) An integrated magnetic resonance plant imager for mobile use in greenhouse and field. *Journal of Magnetic Resonance*. 323: 106879.
Meixner, M., Tomasella, M., Foerst, P., and Windt, C.W. (2020) A small-scale MRI scanner and complementary imaging method to visualize and quantify xylem embolism formation. *New Phytol*. 226: 1517–1529.
Molina-Montenegro, M.A., del Pozo, A., and Gianoli, E. (2018) Ecophysiological basis of the Jack-and-Master strategy: *Taraxacum officinale* (dandelion) as an example of a successful invader. *JPECOL*. 11: rtw121.
Mooney, S.J., Pridmore, T.P., Helliwell, J., and Bennett, M.J. (2012) Developing X-ray Computed Tomography to non-invasively image 3-D root systems architecture in soil. *Plant Soil*. 352: 1–22.
Moreno-Gutiérrez, C., Dawson, T.E., Nicolás, E., and Querejeta, J.I. (2012) Isotopes reveal contrasting water use strategies among coexisting plant species in a Mediterranean ecosystem. *New Phytologist*. 196: 489–496.
Musse, M., De Franceschi, L., Cambert, M., Sorin, C., Le Caherec, F., Burel, A., et al. (2013) Structural Changes in Senescing Oilseed Rape Leaves at Tissue and Subcellular Levels Monitored by Nuclear Magnetic Resonance Relaxometry through Water Status. *Plant Physiol*. 163: 392–406.
Musse, M., Leport, L., Cambert, M., Debrandt, W., Sorin, C., Bouchereau, A., et al. (2017) A mobile NMR lab for leaf phenotyping in the field. *Plant Methods*. 13: 53.
Nagata, A., Kose, K., and Terada, Y. (2016) Development of an outdoor MRI system for measuring flow in a living tree. *Journal of Magnetic Resonance*. 265: 129–138.
Nuixe, M., Traoré, A.S., Blystone, S., Bonny, J.-M., Falcimagne, R., Pagès, G., et al. (2021) Circadian Variation of Root Water Status in Three Herbaceous Species Assessed by Portable NMR. *Plants*. 10: 782.
Pflugfelder, D., Metzner, R., van Dusschoten, D., Reichel, R., Jahnke, S., and Koller, R. (2017) Non-invasive imaging of plant roots in different soils using magnetic resonance imaging (MRI). *Plant Methods*. 13: 102.
Picon-Cochard, C., Pilon, R., Tarroux, E., Pagès, L., Robertson, J., and Dawson, L. (2012) Effect of species, root branching order and season on the root traits of 13 perennial grass species. *Plant Soil*. 353: 47–57.
Pohlmeier, A., Oros-Peusquens, A., Javaux, M., Menzel, M.I., Vanderborght, J., Kaffanke, J., et al. (2008) Changes in Soil Water Content Resulting from *Ricinus* Root Uptake Monitored by Magnetic Resonance Imaging. *Vadose Zone Journal*. 7: 1010–1017.
Pol, M., Schmidtke, K., and Lewandowska, S. (2021) *Plantago lanceolata* – An overview of its agronomically and healing valuable features. *Open Agriculture*. 6: 479–488.
Prieto, I., Roumet, C., Cardinael, R., Dupraz, C., Jourdan, C., Kim, J.H., et al. (2015) Root functional parameters along a land-use gradient: evidence of a community-level economics spectrum. *J Ecol*. 103: 361–373.
Reich, P.B. (2014) The world-wide 'fast–slow'plant economics spectrum: a traits manifesto. *Journal of Ecology*. 102: 275–301.

Rieger, M., and Litvin, P. (1999) Root system hydraulic conductivity in species with contrasting root anatomy. *Journal of Experimental Botany*. 50: 201–209.
Roumet, C., Birouste, M., Picon-Cochard, C., Ghestem, M., Osman, N., Vrignon-Brenas, S., et al. (2016) Root structure–function relationships in 74 species: evidence of a root economics spectrum related to carbon economy. *New Phytol*. 210: 815–826.
Sibgatullin, T.A., Vergeldt, F.J., Gerkema, E., and Van As, H. (2010) Quantitative permeability imaging of plant tissues. *Eur Biophys J*. 39: 699–710.
Signarbieux, C., and Feller, U. (2012) Effects of an extended drought period on physiological properties of grassland species in the field. *J Plant Res*. 125: 251–261.
Terada, Y., Horikawa, Y., Nagata, A., Kose, K., and Fukuda, K. (2020) Dynamics of xylem and phloem sap flow in an outdoor zelkova tree visualized by magnetic resonance imaging. *Tree Physiology*. 40: 290–304.
Van As, H. (2007) Intact plant MRI for the study of cell water relations, membrane permeability, cell-to-cell and long distance water transport. *Journal of Experimental Botany*. 58: 743–756.
Wahl, S., and Ryser, P. (2000) Root tissue structure is linked to ecological strategies of grasses. *New Phytologist*. 148: 459–471.
Washburn, K.E. (2014) Relaxation mechanisms and shales. *Concepts in Magnetic Resonance Part A*. 43A: 57–78.
Westoby, M., Falster, D.S., Moles, A.T., Vesk, P.A., and Wright, I.J. (2002) Plant Ecological Strategies: Some Leading Dimensions of Variation Between Species. *Annu Rev Ecol Syst*. 33: 125–159.
Whittall, K.P., and MacKay, A.L. (1989) Quantitative interpretation of NMR relaxation data. *Journal of Magnetic Resonance (1969)*. 84: 134–152.
Windt, C.W., Vergeldt, F.J., De Jager, P.A., and Van As, H. (2006) MRI of long-distance water transport: a comparison of the phloem and xylem flow characteristics and dynamics in poplar, castor bean, tomato and tobacco. *Plant Cell Environ*. 29: 1715–1729.
Zarebanadkouki, M., Kim, Y.X., and Carminati, A. (2013) Where do roots take up water? Neutron radiography of water flow into the roots of transpiring plants growing in soil. *New Phytol*. 199: 1034–1044.
Zhou, M., Bai, W., Li, Q., Guo, Y., and Zhang, W.-H. (2021) Root anatomical traits determined leaf-level physiology and responses to precipitation change of herbaceous species in a temperate steppe. *New Phytologist*. 229: 1481–1491.
Zhou, M., Guo, Y., Sheng, J., Yuan, Y., Zhang, W., and Bai, W. (2022) Using anatomical traits to understand root functions across root orders of herbaceous species in a temperate steppe. *New Phytologist*. 234: 422–434.

STATEMENTS & DECLARATIONS

Author contributions

A.S.T., G.P. and C.P.-C. designed the research; A.S.T. and C.P.-C. supervised the experiments; M.N., A.S.T., S.B. and C.P.-C. performed the experiments; M.N., A.S.T., G.P. and C.P.-C. analyzed the data; M.N., A.S.T., S.B., J.-M.B., G.P. and C.P.-C. wrote the manuscript.

Email addresses: magali.nuixe@icr.ac.uk (M.N.); amidou.traore@inrae.fr (A.T.); shannan.blystone@inrae.fr (S.B.); jean-marie.bonny@inrae.fr (J.-M.B.); guilhem.pages@inrae.fr (G.P.); catherine.picon-cochard@inrae.fr (C.P.-C.)

Funding

The research leading to these results received funding from the French government IDEX-ISITE initiative 16-IDEX-0001 (CAP 20-25) through the M.N.'s PhD grant and from the ANR project OutLabMRI (ANR-19-CE04-0006).

Competing interest

The authors have no relevant financial or non-financial interests to disclose.

Data availability

The datasets generated during and/or analyzed during the current study are available in the "entrepot.recherche.data.gouv.fr" repository, https://doi.org/10.57745/KPHHAO